HEFAT2014
10th International Conference on Heat Transfer, Fluid Mechanics and Thermodynamics
14 – 16 July 2014
Orlando, Florida

DEVELOPMENT OF A HEATING DEVICE USING CPV AND HEAT PIPE

Dong Il Lee, Geun Seob Oh and Seung Wook Baek*
*Author for correspondence
School of Mechanical, Aerospace and System Engineering, Division of Aerospace Engineering,
Korea Advanced Institute of Science and Technology,
373-1 Guseong-Dong, Yuseong-Gu, Daejeon,
Korea,
E-mail: swbaek@kaist.ac.kr

ABSTRACT

The purpose of this research was to increase the generating efficiency of CPV within a restricted area using solar tracking and heat pipe. At the same time, we demonstrated that the proposed system had the ability to extract thermal energy from a CPV using thermal absorbers containing heat pipe, which could then be used for a heating system or hot-water supply.

Tracking the sun, calculating the sun's position, reinstating the heating device towards the east again for the next day's tracking, and system shutdown were programmed using Simulink. A comparison of the experimental results with KASSI(Korea Astronomy & Space Science Institute) mathematical data for the sun's position confirmed that the algorithm used for the solar-tracking device was correct.

As this system can collect heat from the CPV, the efficiency was much higher than that obtained using air cooling. We performed parametric analysis of the concentration ratio with respect to the operating temperature of the CPV and outlet temperature. The simulated and experimental results for the thermal absorber containing heat pipe were in good agreement.

INTRODUCTION

Solar cells are a popular solution to replace limited conventional energy sources [1]. A new type of solar cell consisting of concentrated photovoltaic (CPV) technology has been developed recently. CPV devices are fabricated using Groups 3–5 compound semiconductors from the periodic table and consist of several layers containing substances from Groups 3 (Ga, In, Al) and 5 (P, As). Because CPVs are accumulated using several different layers, the cell can absorb a wide range of incident light, and thus its efficiency is much higher than that of other types of solar cells [2]. However, for high efficiency, CPV technology requires a solar-tracking device and a cooling system [3].

A solar-tracking device is essential for CPV technology because maximum efficiency is obtained when the orientation of the CPV plane is perpendicular to the incident light. If the angle between the sun and the CPV device is not perpendicular, then the light becomes out of focus, which significantly decreases the efficiency of the device. A cooling system is also necessary for CPV devices, as their electrical efficiency is related to the temperature of the CPV. The efficiency of a CPV device decreases as its operating temperature increases due to the concentration of light. Because CPVs are installed and operated in regions where the sunlight is strong, their temperatures usually rise above 200℃, so cooling is required to raise the efficiency by decreasing the temperature. Many methods of cooling such as natural convection fins have been introduced in the past, but they have not been efficient because they waste a large amount of the heat from the CPV device [4]. In recent years, heating systems have been developed that use air [5]. However, these devices are also inefficient due to the lack of light concentration and their inability to track the sun [6].

The idea behind the present research was to solve the above problems by implementing a heating system that uses water as a coolant to recycle leftover heat. The water passing through the CPVs absorbs heat. A heating system containing a large amount of heat energy can also be operated as a boiler or a turbine. Heat pipes can be used with the heating system to increase the efficiency further. Heat pipes have extremely high thermal conductance during steady-state operation, unlike conventional heat-transfer methods such finned heat sinks. Heat pipes can be used to transfer heat from a heat source, such as a CPV device, to a thermal absorber and water.

This research had three objectives. The first was to design a solar-tracking device that is both sensor and program based, which is essential to maximize the efficiency of CPV devices. The second objective was to improve the electrical efficiency of CPV devices and the thermal efficiency of a thermal absorber by using heat pipes. The third objective was to assess whether the proposed system is practical for use as a heating system or hot water supply by considering a system consisting of 16 connected CPV devices.

NOMENCLATURE

A_o	[m^2]	CPV area
C_p	[J/kgK]	Specific heat capacity of the water
d	[m]	Diameter of the CdS sensor
ha	[hour]	Difference between the actual time and the time for the meridian altitude
H	[m]	Height of the cylindrical housing
k	[W/mK]	Heat transfer coefficient
$\dot{m}$	[kg/s]	Mass flow rate of the water
n	[rad]	Angle of the sun in the absolute coordinate system
$\dot{q}_{irr}$	[W/m^2]	Energy density
T_{in}	[K]	Absorber inlet water temperature
T_{out}	[K]	Absorber outlet water temperature

Special characters

α	[-]	CPV absorptivity
τ	[-]	Lens transmissivity
n_{elec}	[%]	Electrical efficiency
n_{th}	[%]	Thermal efficiency
u	[m/s]	x-component of the water flow velocity
v	[m/s]	y-component of the water flow velocity
w	[m/s]	z-component of the water flow velocity

Subscripts

CR	[-]	Lens concentration ratio
HA	[rad]	Hour angle
LST	[deg]	Local standard time
Te	[min]	Time equation
Tm	[hour]	Time at the meridian altitude

EXPERIMENTAL SET-UP

System Diagram

Figure 1 shows a schematic diagram for the proposed heating system using CPV devices. The system is composed of three parts: a positioner, the CPV devices, and a thermal absorber. The positioner tracks the sun, the CPV generates electricity based on the light concentration obtained while tracking the sun, and the thermal absorber extracts thermal energy from the CPV devices using cooling water.

A triple-junction-based CPV device (Emcore Co., USA) 10 mm in length and width was used for this research. The raw material of the CPV device consisted of InGaP, InGaAs, and Ge. A Fresnel lens with a 290-mm focal length (Fresnel Factory, South Korea), 200 mm in length and width, was used. The solar power was measured using a TM-207 meter (Tenmars Electronics Co., Taiwan), which had an average error of ±1 W/m^2.

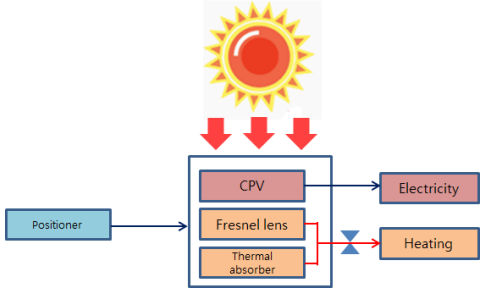

Figure 1 Schematic diagram of a heating system using CPV devices

The CPV device used several wavelengths; thus, a Fresnel lens was required to obtain the desired light concentration. The solar-tracking device was necessary to ensure that the orientation of the CPV plane was perpendicular to the incoming light. If the angle of the sun were not perpendicular to the CPV, the light would be out of focus, thereby significantly degrading the electricity generation.

Figure 2 shows the insulated thermal absorber used for this study, which was constructed from aluminum (width: 80 mm; length: 50 mm; height: 30 mm) and included a CPV device. The CPV device (width: 10 mm; length: 10 mm) was placed on top of the thermal absorber. Thermal grease (ZT100, ZEROtherm Co., South Korea) was used to attach the CPV to the thermal absorber. The 6-mm-diameter inlet and outlet of the thermal absorber were located on the left and right sides, respectively. Two heat pipes using water as the working fluid were located inside the thermal absorber and below the CPV. The length and diameter of each heat pipe were 70mm and 6 mm respectively. The thermal absorber was insulated with glass wool to prevent thermal loss. The total volume flow rate was 200 cc min^{-1}. A K thermocouple was used to measure the water temperature at the inlet and outlet.

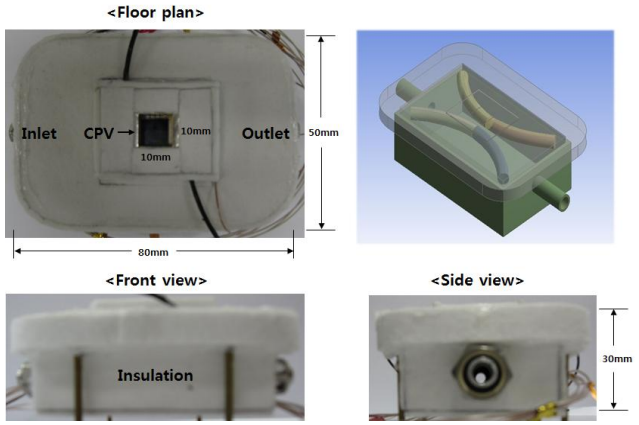

Figure 2 Insulated thermal absorber with a CPV device

Overall Control System

The control system can be described as follows. A Simulink program was used to calculate the azimuthal and elevation angles of the sun using the signals received at 1-second intervals from two solar sensors for the azimuthal angle and two solar sensors for the elevation angle. When the weather was cloudy, the position of the sun was calculated using astronomical and mathematical formulae. After determining the location of the sun, the Simulink program sent signals to control the elevation and azimuthal angles of the heating system using motors.

Solar-tracking Device

Figure 3 shows the configuration of the solar-tracking device, which consisted of a controller, two stepping motors, and four CdS sensors. The controller used Simulink to calculate the sun position and operate the stepping motors, as described in the previous section. Stepping motors are commonly used in precision positioning-control applications; a

stepping motor is brushless and load independent, and it has open-loop positioning capability, good holding torque, and excellent response characteristics. The stepping motor used in the prototype had specifications of 24 V, 0.072° per step, and five phases. The voltage of the CdS sensor changed with the brightness of the light. Depending on the position of the sun, the cylindrical pillar had differing shadows. On the outside of the cylinder, the north-, south-, east-, and west-facing CdS sensors detected the brightness of the ambient light. The voltage values, which varied with the brightness of the light, were supplied to an analog-to-digital converter. Of the four CdS sensors (labeled A, B, C, and D), A and B were used to detect the azimuthal angle, while C and D were used to detect the elevation angle of the sun.

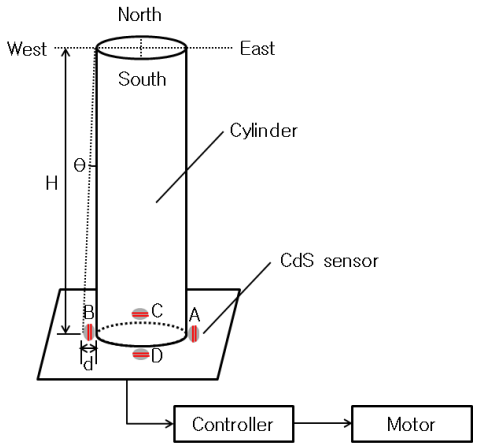

Figure 3 Schematic diagram of the solar-tracking device

The cylindrical housing height was calculated as follows. If H is the height of the cylindrical housing, d is the diameter of the CdS sensor, and θ is the angle of the shadow formed by the cylindrical pillar, we have $\tan\theta = \frac{d}{H}$. If the angle of the shadow is 1°, H can be obtained from $H = \frac{d}{\tan 1^o} = \frac{0.003}{0.017} = 0.176m$. If a CdS sensor (R1) and a resistor (R2) are connected to a circuit voltage, the output voltage can be calculated by the following expression: $V_{out} = \frac{R2}{R2+R1} \cdot V_{in}$. Based on this equation, the output voltage increases in bright places because of the reduced resistance of R1 and decreases in dark places due to the increased resistance of R1.

Algorithms

When CdS sensors located on the east and west sides detect voltages, the average voltage of the two CdS sensors is compared against a threshold value. As the sun moves to the west, shadows are formed on the east side. The reduced light causes the voltage of the east-side CdS sensor to decrease relative to that of the west-side CdS sensor. If the voltage on the east side is less than the threshold of the average azimuthal voltage and greater than the cloudy threshold, the condition is set to a true value; if not, the condition is set to a false value. The error of each CdS sensor is less than 0.2% for a voltage supply of 5 V. The system moves to track the sun when the difference between the voltage of the two sensors is more than 0.01 V (0.2% of 5 V). The same algorithm is used to control the elevation angle based on signals from the north-side and south-side CdS sensors.

If the average voltage obtained from the two sensors is less than the cloudy threshold for a given second, solar tracking is carried out by a program that calculates the position of the sun using astronomical and mathematical formulae. The program uses the current time and the actual location (longitude and latitude) of the solar-tracking device. First, the time data are gathered using the "clock" and "fix" functions, where y is years, m is months, d is days, h is hours, mi is minutes, and s is seconds. Second, the angle of the sun is calculated in the absolute coordinate system using

$$\mathrm{n} = \frac{2\mathrm{pi}}{365}\left(da - 1 + \frac{h}{24} + \frac{mi}{1440} + \frac{s}{86400}\right) \quad (1)$$

where da is the number of days calculated from the beginning of the year [7]. For instance, da is 31 + 4 = 35 for February 4. Therefore, n is the absolute angle through which the sun has rotated. For example, n is 2 pi (= 360°) for December 31 at 24 hours, 0 minutes, 0 seconds. Third, the position of the sun is calculated using the equator coordinate system. For the declination (dec) in radians [8],

$$\begin{aligned}\mathrm{dec} &= 0.006918 - 0.399912\cos(\mathrm{n}) \\ &+ 0.070257\sin(\mathrm{n}) - 0.006758\cos(2\mathrm{n}) \\ &+ 0.000907\sin(2\mathrm{n}) - 0.002697\cos(3\mathrm{n}) + 0.00148\sin(3\mathrm{n})\end{aligned} \quad (2)$$

For the hour angle (HA) in radians,

$$\mathrm{HA} = \frac{\mathrm{pi}}{180} \bullet 15 \bullet 24\left(\frac{\mathrm{ha}}{24} - \mathrm{floor}\left(\frac{\mathrm{ha}}{24}\right)\right) \quad (3)$$

where ha is the difference between the actual time and the time at the meridian altitude (Tm):

$$\mathrm{ha} = 24 + \left(\mathrm{h} + \frac{\mathrm{mi}}{60} + \frac{\mathrm{s}}{3600} - \mathrm{Tm}\right) \quad (4)$$

$$\mathrm{Tm} = 12 + \frac{4\mathrm{L} - \mathrm{Te}}{60} \quad (5)$$

Here, *L* is related to local standard time (LST)

$$\mathrm{L} = \mathrm{LST} - \mathrm{longitude(actual)} \quad (6)$$

and *Te* is the equation for time, which can be determined from

$$\mathrm{A} = \frac{360}{365.24}(\mathrm{d} + 9) \quad (7)$$

$$\mathrm{B} = \frac{\mathrm{pi}}{180}\left(\mathrm{A} + \frac{360 \bullet 0.0167}{\mathrm{pi}}\sin\left(\frac{\mathrm{pi}}{180} \bullet \frac{360}{365.24} \bullet (\mathrm{d} - 3)\right)\right) \quad (8)$$

$$\mathrm{C} = \left(\mathrm{A} - \frac{180}{\mathrm{pi}} \bullet a\tan(\tan(\mathrm{B}) / \cos(\frac{\mathrm{pi} \bullet 23.44}{180}))\right) / 180 \quad (9)$$

$$\mathrm{Te} = 720(\mathrm{C} - \mathrm{floor}(\mathrm{C} + 0.5)) \quad (10)$$

Finally, the position of the sun is calculated in the horizontal coordinate system [7]. For the altitude (*alt*) in radians,

$$\text{alt} = \text{asin}(\sin(\text{lat}) \bullet \sin(\text{dec}) + \cos(\text{lat}) \bullet \cos(\text{dec}) \bullet \cos(\text{H})) \quad (11)$$

For the azimuthal angle (*azi*) in radians,

$$(\text{h} < \text{Tm})\ \text{azi} = \text{acos}((\sin(\text{dec}) \bullet \cos(\text{lat}) - \cos(\text{dec}) \bullet \sin(\text{lat}) \bullet \cos(\text{H}))/\cos(\text{alt})) \quad (12)$$

$$(\text{h} \geq \text{Tm})\ \text{azi} = \text{acos}((\sin(\text{alt}) \bullet \sin(\text{lat}) - \sin(\text{dec}))/(\cos(\text{alt}) \bullet \cos(\text{lat}))) + \text{pi} \quad (13)$$

In the research described in this paper, we used longitude = 127.42°, latitude = 36.35°, and LST = 135°.

The sun was tracked by activating the motor to move the heating system toward the west until the output voltages of CdS sensors A and B (azimuthal) were similar. The same control algorithm was used for the elevation angle.

The procedure for calculating the azimuthal or elevation angle was as follows. First, the number of pulses was calculated as the motor operated clockwise. Second, the clockwise angle was computed by multiplying the number of pulses by the per pulse angle of the moving motor. Third, the clockwise rotation angle was calculated by subtracting the counterclockwise angle. Finally, the azimuthal angle was obtained by adding the initial azimuthal angle. The same calculation algorithm was used for the elevation angle.

The procedure for shutting down the system was as follows. CdS sensors located on the east, west, south, and north sides detected the voltage depending on the brightness of the light. The averages of the four voltage values were compared against a shutdown threshold; if they were less than the shutdown threshold, a true value was generated; otherwise, a false value was generated. If a true value was obtained, an algorithm was used to calculate the number of pulses to reposition the device toward the east, and the system was shut down.

The number of pulses to reposition the device toward the east was calculated as follows. First, the initial azimuthal angle was subtracted from the final azimuthal angle. Second, the number of pulses for repositioning the azimuth was obtained by dividing the angle per pulse of the moving motor by the above azimuthal angle. The same algorithm was used to calculate the number of pulses to reposition the elevation angle. Repositioning the solar-tracking device and heating system to the east after sunset allowed for efficient tracking of the sun at sunrise on the next day.

RESULTS AND DISCUSSION

Verification of the Solar-tracking System

The solar-tracking system underwent extensive testing for this study. Figure 4(a) shows the transient motion of the heating system for every hour, on the hour. The right and left sides of each figure correspond to the eastward and westward directions, respectively. The solar sensor of the heating system moved from east to west while tracking the trajectory of the sun. After sunrise, the solar sensor searched for the sun automatically. Tracking of the sun was also initiated after the disappearance of cloud cover. After sunset, the solar sensor was shut down automatically.

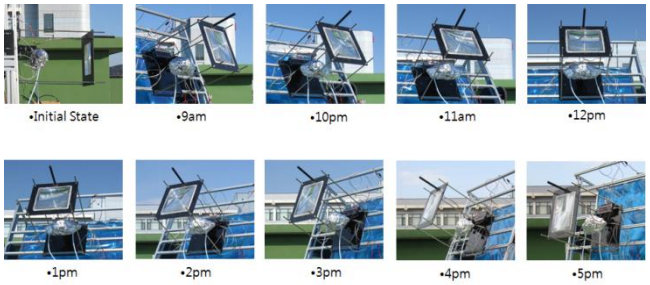

Figure 4(a) Transient motion of the heating system as a function of time

The experimental azimuthal and elevation angles registered at the Korea Advanced Institute of Science and Technology (KAIST) were compared with the actual values obtained from the Korea Astronomy and Space Science Institute (KASSI) [9-11]. The average error between 9:00 am and 5:00 pm was within 0.04°, as shown in Fig. 4(b). According to these results, the solar-tracking algorithm used for the heating system was accurate.

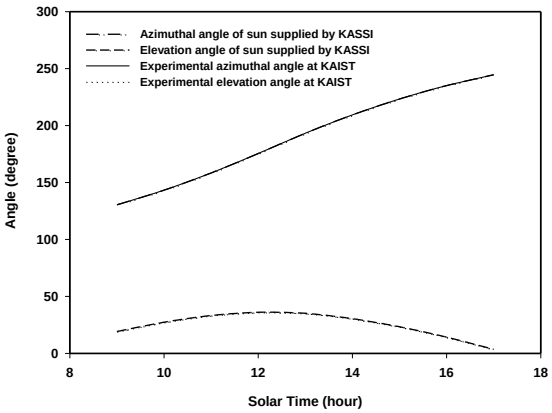

Figure 4(b) Comparison of the actual values obtained from KASSI with experimental data

Electrical and Thermal Efficiency

The total energy (Q_1), maximum power (P), collected heat (Q_2), electrical efficiency (n_{el}), and thermal efficiency (n_{th}) are given below:

$$Q_1 = \tau \bullet \alpha \bullet A_0 \bullet CR \bullet q''_{irr} \quad (14)$$

$$P = VI \quad (15)$$

$$Q_2 = \dot{m} C_p (T_{out} - T_{in}) \quad (16)$$

$$n_{elec} = \frac{P}{Q_1} \times 100(\%) \quad (17)$$

$$n_{th} = \frac{Q_2}{Q_1} \times 100(\%) \quad (18)$$

For this study, the lens concentration ratio (CR) was 400, the lens transmissivity (τ) was 0.9, and the CPV absorptivity (α) was 0.9. Here, q''_{irr} represents the energy density, A_0 is the CPV area, $\dot{m}$ represents the mass of the water, C_p is the specific heat capacity of the water, T_{in} is the absorber inlet temperature, and T_{out} is the absorber outlet temperature of the water.

Figure 5 shows the electrical and thermal efficiencies of the CPV with or without heat pipes as a function of time. The average electrical efficiency with heat pipes was ~20% during the day, slightly higher than the efficiency without heat pipes (~19%). The average thermal efficiencies with and without heat pipes were 77% and 75% respectively. Therefore, the electrical efficiency of the CPV device and the thermal efficiency of the thermal absorber were improved by using heat pipes. The proposed system demonstrated 97% total efficiency (electrical + thermal). Because this system could collect heat from the CPV device, its efficiency was much greater than that of other renewable energy systems. On average, changes in the electrical efficiency were minimal. Also, the thermal efficiency was constant, irrespective of time and outside temperature, because the thermal absorber was insulated with glass wool.

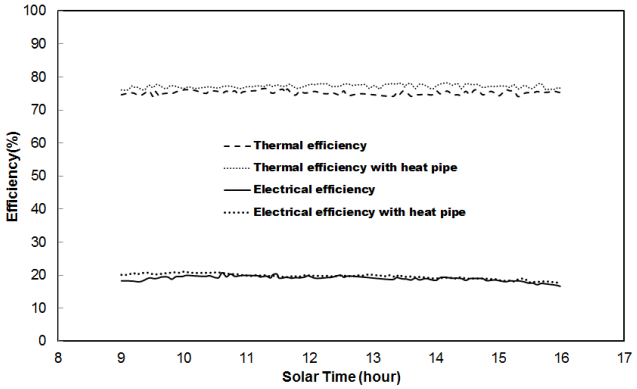

Figure 5 Electrical and thermal efficiencies of a CPV device and thermal absorber with and without heat pipes as a function of solar time

Verification of the Heating System Using a CPV Device

For CPV devices, the sunlight is typically concentrated by mirrors or lenses. A lens concentrates the sunlight onto the CPV device to increase the light density at the CPV surface. The CPV device reaches its steady-state temperature when the luminous power absorbed is equivalent to the sum of the electric power delivered to the load plus the power obtained in the form of heat. When thermal equilibrium is reached, the conservation equation for the CPV device is as follows:

$$\tau\alpha A_0 CR q''_{irr} - \eta_{elec}\tau\alpha A_0 CR q''_{irr} - \dot{m}C_P(T_{out} - T_{in}) = 0 \quad (19)$$

where the first term in Eq. (19) denotes the luminous power absorbed by the CPV due to the lens transmissivity (τ), and α is the CPV surface absorptivity, A_0 is the CPV area, CR is the lens geometric concentration ratio, and q''_{irr} is the energy density. The second term in the equation represents the electric power delivered to the external load, where η is the conversion efficiency. The last term represents the heat obtained from the thermal absorber by the water.

The flow of water inside the thermal absorber was assumed to be incompressible and steady state. Thus, the mass balance equation is given as

$$\frac{\partial\rho}{\partial t} + \frac{\partial(\rho u)}{\partial x} + \frac{\partial(\rho v)}{\partial y} + \frac{\partial(\rho w)}{\partial z} = 0 \quad (20)$$

where ρ is the density of water, and u, v, and w represent the x-, y-, and z-components of the water-flow velocity.

The momentum equations in the x, y, and z directions are then expressed as

$$\rho\frac{Du}{Dt} = -\frac{\partial p}{\partial x} + \frac{\partial\tau_{xx}}{\partial x} + \frac{\partial\tau_{yx}}{\partial y} + \frac{\partial\tau_{zx}}{\partial z} + F_x \quad (21)$$

$$\rho\frac{Dv}{Dt} = -\frac{\partial p}{\partial y} + \frac{\partial\tau_{xy}}{\partial x} + \frac{\partial\tau_{yy}}{\partial y} + \frac{\partial\tau_{zy}}{\partial z} + F_y \quad (22)$$

$$\rho\frac{Dw}{Dt} = -\frac{\partial p}{\partial z} + \frac{\partial\tau_{xz}}{\partial x} + \frac{\partial\tau_{yz}}{\partial y} + \frac{\partial\tau_{zz}}{\partial z} + F_z \quad (23)$$

where p is the pressure on the water element, τ_{xx}, τ_{xy}, and τ_{xz} are the viscous forces, and F_x, F_y, and F_z are the volume forces. The energy balance equation is given as

$$\frac{\partial(\rho T)}{\partial t} + \frac{\partial(\rho u T)}{\partial x} + \frac{\partial(\rho v T)}{\partial y} + \frac{\partial(\rho w T)}{\partial z} = \frac{\partial}{\partial x}\left[\frac{k}{C_p}\frac{\partial T}{\partial x}\right] + \frac{\partial}{\partial y}\left[\frac{k}{C_p}\frac{\partial T}{\partial y}\right] + \frac{\partial}{\partial z}\left[\frac{k}{C_p}\frac{\partial T}{\partial z}\right] + S_T \quad (24)$$

where C_p is the specific heat, T is the temperature, k is the heat transfer coefficient, and S_T is the heat source (i.e., solar radiation energy received from the CPV).

The performance of the heating system was analyzed using a numerical model. The energy density was 1,230 W/m^2 measured using a solar power meter. The volume flow rate was 200 cc min^{-1}, and the inlet temperature was 9.6℃. The heat flux of the CPV was calculated for a lens concentration ratio (CR) of 400. The thermal conductivity of the heat pipe was 15,000 W/m·K. The heat pipe was treated as a solid material with extremely high thermal conductivity, and the value was estimated based on experimental data. The values used for the Fresnel lens transmissivity and the CPV's surface absorptivity were 0.9. As this experiment was performed for insulated conditions, the temperature of the atmosphere was not important. The Reynolds number was about 540, so a laminar model was used. The number of nodes was 159,931. The maximum and minimum sizes of the mesh were 1.41 × 10^{-2} m and 7.07 × 10^{-5} m, respectively. The maximum skewness was 0.91, and the minimum orthogonal quality was 0.21. Hexahedral and tetrahedral elements were used.

Figure 6 shows the temperature distribution on the interface of the CPV device and the thermal absorber with heat pipes. The simulation gave a maximum CPV surface temperature of 25.3℃. The upper face of thermal absorber (located 20mm from the right end of the CPV device) toward the outlet had a temperature of 17.7℃, and the average outlet water temperature was 11.9℃. The experimental temperatures measured using a K thermocouple were 16.9℃ for the upper

face and 11.8℃ for the average water temperature, demonstrating good agreement between the simulation and experiment.

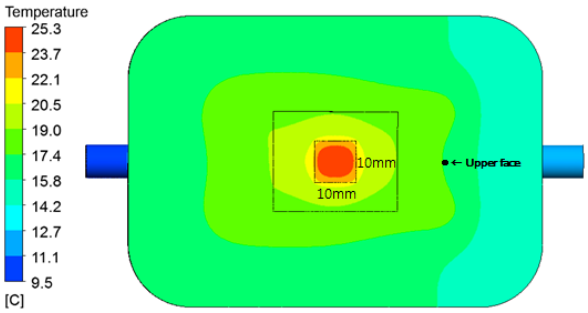

Figure 6 Temperature distribution on the interface of a CPV device and thermal absorber with heat pipes

Table 1 shows the simulated temperatures of the CPV device and the thermal absorber with heat pipes for different lens concentration ratios. As the lens concentration ratio increased from 500 to 800, the outlet temperature increased from 12.5 to 14.2℃. This means that a higher concentration ratio generated more hot water per hour under the same inlet conditions. However, the change in the thermal efficiency was small according to Eqs. (16) and (18). The average thermal efficiency was 80%. The CPV temperature increased from 29.3 to 41.2℃ as the amount of solar radiation increased.

Table 1 Simulated temperatures of the CPV device and the thermal absorber with heat pipes for different lens concentration ratios

Concentration ratio	Max. temp. of CPV (^{o}C)	Average temp. at the outlet (^{o}C)
500	29.3	12.5
600	33.3	13
700	37.2	13.6
800	41.2	14.2

Simulation Results of the Heating System Using Multiple CPV Devices

Figure 7 shows the simulation results for a heating system with a CPV grid consisting of 16 connected CPV devices (four horizontal rows and four vertical rows). The CPV grid was attached to a thermal absorber (the same size as shown in Fig. 8). This system could generate electricity from the CPV devices and simultaneously supply hot water collected from the CPV devices, which was heated by the thermal absorber. The lens concentration ratio was 400, and the distance between the CPV devices was 200 mm. The following values were used to simulate the same conditions that were modeled for Fig. 6: volume flow rate of 200 cc min^{-1} and inlet temperature of 9.6℃.

The inlet and outlet were located at the bottom left and right corners, respectively. The maximum temperature of the CPV grid was 58.5℃, and the average temperature at the outlet was 45.2℃. These temperature results are suitable for CPV operation as well as for heating and supplying hot water. Note that if the thermal absorber were not insulated, then the outlet temperature of the heating system would decrease due to increased radiation and convection.

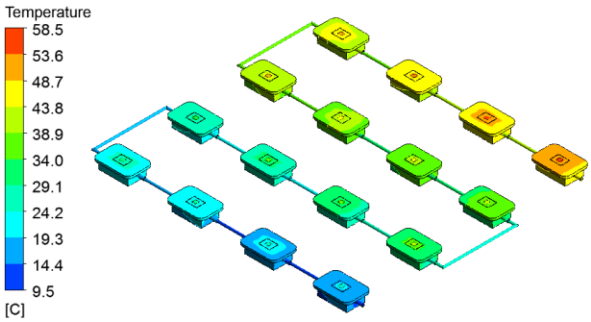

Figure 7 Heating system using a CPV grid

Validation of the Heating System using Multiple CPV Devices

Figure 8 shows a validation of the heating system using a CPV grid consisting of 16 connected CPV devices (four horizontal rows and four vertical rows). The solar sensor located on the upper side of the heating system moved from east to west while tracking the trajectory of the sun. The inlet and outlet were located at the bottom left and right corners, respectively.

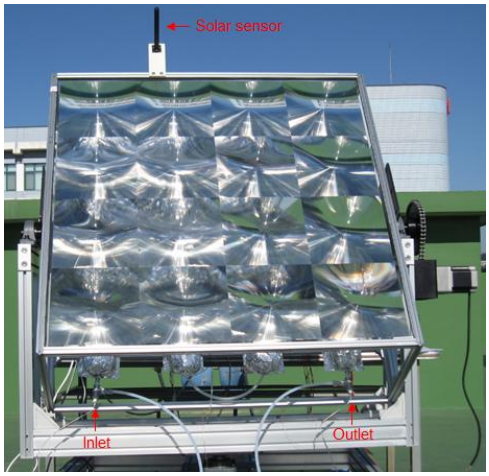

Figure 8 Validation of the heating system using a CPV grid

The average electrical efficiency was ~20% during the day, and the average thermal efficiency was 72%. Therefore, the proposed system had a total efficiency (electrical + thermal) of 92%. On average, changes in the electrical efficiency were minimal whereas the difference between each of the electrical efficiency was within 1%. Moreover, the thermal efficiency was constant, irrespective of time and outside temperature because the thermal absorber was insulated with glass wool. The experimental temperatures were measured using a K

thermocouple. The average water temperature measured at the outlet was 40.8℃, which was in good agreement with the simulation.

Therefore, this system could generate electricity from the CPV devices, and simultaneously supply hot water collected from the CPV devices, which was heated by the thermal absorber. Because this system could collect heat from the CPV devices, its efficiency was much higher than that of other renewable energy systems.

CONCLUSION

An efficient heating system using CPV devices with heat pipes was developed. The electrical efficiency of the CPV devices was increased by using concentrated light and solar tracking, and the thermal energy from the CPV devices was extracted to increase the thermal efficiency of the heating system. With this system, we were able to supply hot water using a thermal absorber to collect the heat from the CPV devices.

Simulink was used to track the sun, calculate the sun's position, reposition the heating system toward the east again after sunset for the next day's tracking, and shut the system down. When the weather was cloudy, the position of the sun was calculated using astronomical and mathematical formulae. A comparison of the experimental results with KASSI mathematical data for the position of the sun confirmed that the algorithm used for the solar-tracking device was accurate; the average error was within 0.04° between 9:00 am and 5:00 pm.

The average electrical efficiency was 20% during the day, much higher than the efficiency of commonly used silicon solar cells (13% efficiency). The average thermal efficiency was 77%. Therefore, this system had a total efficiency (electrical + thermal) of 97%. Since this system could also collect heat from the CPV devices, the efficiency was much higher than that of other renewable energy systems. The simulated and experimental results for the thermal absorber were in good agreement.

When the concentration ratio increased, so did the outlet temperature. However, the change in thermal efficiency was relatively small compared with the increase in the concentration ratio. The temperature of the CPV devices increased due to an increase in solar radiation energy.

Multiple thermal absorbers were connected to simulate a heating system. The simulated and experimental results for the thermal absorber were in good agreement. This system was capable of generating electricity from the CPV devices while supplying hot water collected from the thermal absorber. The heating system produced more hot water per hour during summer than during winter and also had a higher concentration ratio.

The advantages of a heating system using CPV devices are as follows. The system is economical. Heating and hot water storage are available in the absence of sunlight. The system offers higher generating efficiency than do other renewable energy systems, and it reduces greenhouse gas generation. Moreover, the system exhibits high sustainability when the sun is present.

REFERENCES

[1] Timilsina G.R., Kurdgelashvili L., and Narbel P.A., Solar energy: Markets, economics and policies, *Journal of Renewable and Sustainable Energy*, Vol. 16, 2012, pp. 449–465

[2] Cotal H., Fetzer C., Boisvert J., Kinsey G., King R., Hebert P., Yoon H., and Karam N., III – V multijunction solar cells for concentrator photovoltaics, *Energy and Environmental Science*, Vol. 2, 2009, pp. 174–192

[3] Anja R., Christopher J.D., and David R.M., Cooling of photovoltaic cells under concentrated illumination: A critical review, *Solar Energy Material and Solar Cells*, Vol. 86, 2005, pp. 451–483

[4] Teo H.G., Lee P.S., M.N., and Hawlader A., An active cooling system for photovoltaic modules, *Applied Energy*, Vol. 90, 2012, pp. 309–315

[5] Amori K.E., and Al-Najjar H.M.T., Analysis of thermal and electrical performance of a hybrid (PV/T) air based solar collector for Iraq, *Applied Energy*, Vol. 98, 2012, pp. 384–395

[6] Zogou O., and Stapountzis H., Flow and heat transfer inside a PV/T collector for building application, *Applied Energy*, Vol. 91, 2012, pp. 103–115

[7] Walraven R., Calculating the position of the sun, *Solar Energy*, Vol. 20, 1978, pp. 393–397

[8] Karakoti I., Das P.K., and Bandyopadhyay B., An analytical study on daily solar radiation data, *Current Science*, Vol. 105, 2013, pp. 215–224

[9] Meeus J., Astronomical Algorithms, William-Bell, 1998, Second Edition

[10] Bretagnon P., Theory for the motion of all the planets - The VSOP82 solution, *Astronomy and Astrophysics*, Vol. 114, 1982, pp. 278–288

[11] Bretagnon P., and Francou G., Planetary theories in rectangular and spherical variables - VSOP 87 solutions, *Astronomy and Astrophysics*, Vol. 202, 1988, pp. 309–315